Eur. Phys. J. A **14**, 63–75 (2002)
DOI 10.1140/epja/iepja1387

THE EUROPEAN PHYSICAL JOURNAL A

Nuclear spins, magnetic moments and α-decay spectroscopy of long-lived isomeric states in ^{185}Pb

A.N. Andreyev[1,a], K. Van de Vel[2], A. Barzakh[3], A. De Smet[2], H. De Witte[2], D.V. Fedorov[3], V.N. Fedoseyev[4,b], S. Franchoo[5,6], M. Górska[2,c], M. Huyse[2,5], Z. Janas[7], U. Köster[5], W. Kurcewicz[7], J. Kurpeta[7], V.I. Mishin[4], K. Partes[5], A. Plochocki[7], P. Van Duppen[2], and L. Weissman[5,d]

[1] Department of Physics, Oliver Lodge Laboratory, University of Liverpool, PO Box 147, Liverpool, L69 7ZE, United Kingdom
[2] Instituut voor Kern- en Stralingsfysica, University of Leuven, Celestijnenlaan 200 D, B-3001 Leuven, Belgium
[3] Petersburg Nuclear Physics Institute, 188300, Gatchina, Russia
[4] Institute of Spectroscopy, Russian Academy of Sciences, 142190, Troitsk, Russia
[5] ISOLDE CERN, CH-1211 Genève 23, Switzerland
[6] University of Mainz, D-55099, Mainz, Germany
[7] Institute of Experimental Physics, University of Warsaw, Hoza 69, PL-00681, Warsaw, Poland
IS387 Collaboration and ISOLDE Collaboration

Received: 7 February 2002 / Revised version: 18 February 2002
Communicated by J. Äystö

Abstract. Alpha-decay properties of the neutron-deficient isotope ^{185}Pb were studied at the PSB-ISOLDE (CERN) on-line mass separator using the resonance ionisation laser ion source (RILIS). The nuclei of interest were produced in a 1.4 GeV proton-induced spallation reaction of a uranium graphite target. In contrast to previous studies, two α-decaying isomeric states were identified in ^{185}Pb. The relative production of the isomers, monitored by their α-counting rates, could be significantly changed when a narrow-bandwidth laser at the RILIS setup was used to scan through the atomic hyperfine structure. Based on the atomic hyperfine structure measurements, along with the systematics for heavier odd-mass lead isotopes, the spin and the parity of these states were interpreted as $3/2^-$ and $13/2^+$ and their nuclear magnetic moments were deduced. The α-decay energy and half-life value for the $I^\pi = 13/2^+$ isomer are $E_\alpha = 6408(5)$ keV, $T_{1/2} = 4.3(2)$ s, respectively; while for the $I^\pi = 3/2^-$ isomer ($T_{1/2} = 6.3(4)$ s) two α-decays with $E_{\alpha 1} = 6288(5)$ keV, $I_{\alpha 1} = 56(2)\%$ and $E_{\alpha 2} = 6486(5)$ keV, $I_{\alpha 2} = 44(2)\%$ were observed. By observing prompt α-γ coincidences new information on the low-lying states in the daughter isotope ^{181}Hg was obtained.

PACS. 27.70.+q $150 \leq A \leq 189$ – 23.60.+e Alpha decay – 32.10.Dk Electric and magnetic moments, polarizability – 32.10.Fn Fine and hyperfine structure

1 Introduction

The last decade witnessed a substantial progress in the study of decay properties of very neutron-deficient nuclei around the closed proton shell at $Z = 82$ and neutron mid-shell at $N = 104$. A traditional method to produce such nuclei is the use of high-intensity (up to 10^{12} ions/s) heavy-ion–induced complete fusion reactions close to the Coulomb barrier, see for example [1–4] and references therein. However, in many cases the intensity of the exotic ions which can be obtained with this method suffers from a relatively low target thickness of a few mg/cm^2, which is required to allow the evaporation residue to recoil out of the target and be further investigated.

An alternative to this method is provided by high-intensity (up to 3×10^{13} protons/s) high-energy (up to 1.4 GeV) proton-induced spallation reactions on thick (hundred grams and more) targets made of heavy elements (Pb, Th, U) or their compounds. Unfortunately, this production mechanism is unselective and simultaneously produces hundreds of different exotic nuclei in the target. Therefore, this technique necessarily requires subsequent on-line mass separation. Quite often, even after mass separation, the resulting beams of the exotic nuclei of interest are highly contaminated with much more abundantly produced isobars with different atomic numbers. A

[a] e-mail: aan@ns.ph.liv.ac.uk
[b] *Present address*: ISOLDE CERN, CH-1211 Genève 23, Switzerland.
[c] *Present address*: GSI, Darmstadt, D-64220, Germany.
[d] *Present address*: NSCL, Michigan State University, East Lansing, MI 48824-1321.

recent refinement of this method has been accomplished by the addition of a resonance ionisation laser ion source (RILIS) [5,6] which allows selective ionisation of isotopes of a specific element and therefore provides purer beams after subsequent on-line mass separation.

In the present work we report on an α-decay study of ^{185}Pb, performed by using a RILIS coupled to the ISOLDE on-line mass separator at CERN. Our interest in this nucleus was motivated by the following reasons:

- First of all, only one α-decaying state was identified in ^{185}Pb in two previous α-decay studies [1,2], in contrast to the heavier odd-mass lead isotopes with $A = 187$, 191–203, in which two long-lived isomeric states are known [7]. However, based on systematics and on the results of theoretical predictions, one would expect the presence of a high-spin (presumably, $13/2^+$) and a low-spin (presumably, $3/2^-$) isomer in this nucleus, similar to the neighbouring nucleus ^{187}Pb [8,9]. These states are expected to result from the weak coupling of $1i_{13/2}$ or $3p_{3/2}$ neutrons, respectively, to the spherical even-even lead core. Therefore, possible long-lived ($T_{1/2} \approx$ seconds) isomeric states in ^{185}Pb were searched for in our study.
- The study of atomic hyperfine structure using RILIS can provide information on the magnetic moment and spin of the states under investigation and therefore on the configuration of these states.
- ^{185}Pb is the daughter nucleus of ^{189}Po (after α-decay), which has been recently studied at the velocity filter SHIP [4]. As was shown in [4], ^{189}Po has a rather complex decay pattern to the states in ^{185}Pb and detailed information on the latter nucleus is crucial in order to make unambiguous assignment of the states in the parent isotope ^{189}Po.
- In turn, the α-decay of ^{185}Pb populates low-lying states in the daughter nucleus ^{181}Hg. A recent in-beam γ-decay study of ^{181}Hg [10] provided information on yrast and some non-yrast states, while the current investigation could supply important complementary data on possible low-lying states which could not be populated in the in-beam study.

As mentioned above, prior to our work, the nucleus ^{185}Pb was investigated in α-decay studies, discussed in refs. [1,2]. The first study [1] used a complete fusion reaction ^{150}Sm(^{40}Ca, 5n)^{185}Pb and employed the He gas-jet technique combined with α spectrometry. This study attributed two α-decays to ^{185}Pb with the energies of $E_{\alpha 1} = 6400(10)$ keV, $I_{\alpha 1} \approx 72\%$ and $E_{\alpha 2} = 6480(20)$ keV, $I_{\alpha 2} \approx 28\%$, but no information on the half-life value was given (see table 1 in sect. 3). In the experiment reported in ref. [2], a complete fusion reaction ^{142}Nd(^{48}Ti, 5n)^{185}Pb was used and after ionisation and mass separation with the on-line mass separator at GSI (Darmstadt), the activity was implanted in a thin carbon foil. A rather elaborate detection system then allowed the information on α-decay energies and half-lives to be collected. In addition to the previously reported two α lines from ref. [1], three new α lines were found (see table 1). Based on all five α lines, a half-life value of $T_{1/2} = 4.1(3)$ s was reported, but no spin and parity assignments could be obtained from these experiments. We stress that in [1,2] no evidence for different isomeric states in ^{185}Pb was suggested.

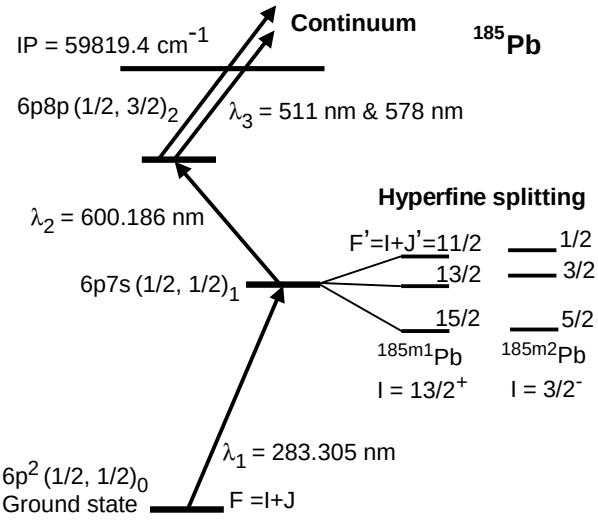

Fig. 1. The three-step laser ionisation scheme for ^{185}Pb, applied in this work. Shown are electronic configurations for the levels involved and laser wavelengths for each step. On the right the schematic illustration of the HFS components in case of the $13/2^+$ and $3/2^-$ isomeric states in ^{185}Pb is presented. More details are given in the text.

The structure of the paper is as follows: in sect. 2 we describe the experimental setup together with the detection system used; sect. 3 presents the experimental data, which are discussed in sect. 4. Conclusions are presented in sect. 5.

2 Experimental setup

2.1 RILIS, isotope production and mass separation

The ^{185}Pb nuclei were produced in a spallation reaction induced by a 1.4 GeV proton beam impinging on a UC_x target (50 g/cm^2 of ^{238}U and ≈ 10 g/cm^2 of carbon) of the ISOLDE mass separator. Two proton pulses (3×10^{13} protons each, spaced by 2.4 s), provided by the PS Booster in each supercycle of 16.8 s, were sent to the ISOLDE target. After production in the target, heated to about 2050°C, the nuclei diffuse mainly as atoms to the hot cavity ($\approx$ 2100°C), made from a niobium tube of 30 mm length and 3 mm internal diameter. Laser beams were focused into the hot cavity, where the resonance ionisation of ^{185}Pb was performed by using a three-step ionisation scheme, shown in fig. 1. The resonant excitation of the first two atomic transitions ($\lambda_1 = 283.305$ nm and $\lambda_2 = 600.186$ nm) was provided by two tunable pulsed dye lasers; the ultraviolet radiation λ_1 was obtained by frequency doubling of the fundamental dye laser radiation with a non-linear BBO crystal. Pumping the dye lasers and excitation of the final ionising transition (the third step) into the continuum were achieved by copper vapour lasers, operating at a pulse repetition rate of 11 kHz.

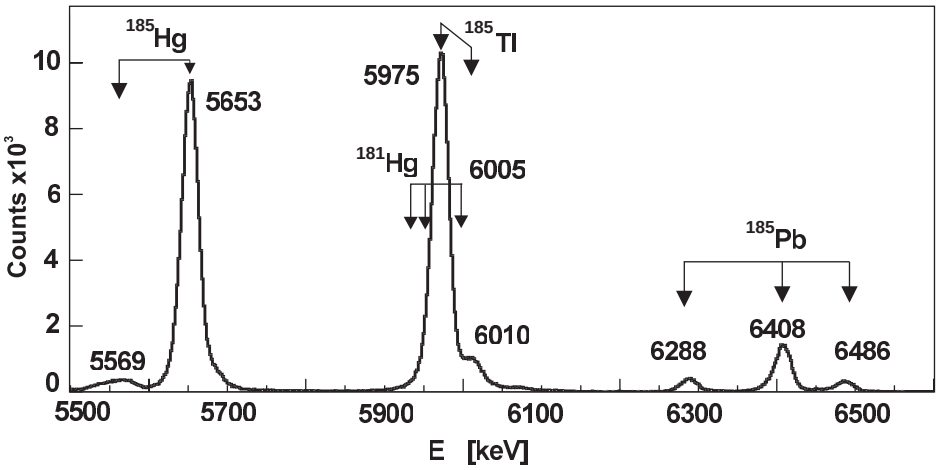

Fig. 2. Energy spectrum of the α-particles measured in the Si-detector with a broad-bandwidth laser in the first excitation step. Some of the α peaks are labelled with the α-decay energy (in keV) and the isotope the α-decay belongs to. The expected positions of the α-decays of ^{181}Hg, being the daughter product of ^{185}Pb, are also shown.

An ionisation efficiency of about 3% was measured in off-line tests with stable lead isotopes [11]. During the on-line experiment with radioactive nuclei the laser power of the ionising step was about a factor of two lower, so we estimate the on-line efficiency for Pb isotopes to be $\approx 1.5\%$. More details on the RILIS and ionisation schemes can be found in [5,6,11].

After resonance ionisation in the hot cavity, the ions were extracted and mass separated in the general purpose separator (GPS) of ISOLDE, tuned to select nuclei with mass $A = 185$. The mass-separated ions were implanted at an angle of 56° into a movable aluminized mylar tape (100 μm thickness, 12.5 mm width) which was surrounded by the detection setup.

2.2 Detection system and modes of measurement

To measure the α-decay of the implanted nuclei a Si-detector with a sensitive area of 450 mm^2 and a thickness of 500 μm was installed inside the vacuum chamber with the tape. The distance between the detector centre and the implantation spot was 28 mm, the detector being inclined at 28°, relative to the tape. To measure γ-rays in coincidence with the α-particles, a Ge-detector was installed outside the vacuum chamber on the opposite side of the tape at a distance of a few cm from the implantation point. No singles γ-ray spectra were recorded.

Data were collected in list-mode by using a data acquisition system, which consisted of two ADCs (analogue-to-digital converter) for the α- and γ-decay energy measurements, a TDC (time-to-digital converter) and a TAC (time-to-amplitude converter) modules. The TDC measured the absolute time between the start of the measurement cycle and detection of any particular event (singles α or α-γ coincident pair) within the range of 15.5 s with a channel width of 10 ms. The reset of the TDC and the start of the measurement cycle were triggered by the first proton pulse coming to the ISOLDE target within every supercycle. The measurement cycle continued for 15.5 s (defined by the TDC range), and after this interval the tape moved within 0.8 s in order to avoid build-up of long-lived background activities and of daughter products of the isotopes of interest. Finally, a TAC was used to measure the time difference between coincident α and γ events within a time interval of 1 μs.

Two different modes of measurement were exploited during this experiment: atomic hyperfine structure (HFS) measurements and nuclear spectroscopic data collection. These modes differed only by the laser bandwidth of the first excitation step: a narrow bandwidth of 1.2 GHz (before frequency doubling) for the HFS measurements and a broad bandwidth of 10 GHz (before frequency doubling) for the spectroscopic data collection. The data collected during the HFS measurements were also used for the spectroscopic study. The next sections present detailed explanations of these measurements.

3 Experimental procedure and data analysis

Figure 2 shows the energy spectrum of α-particles measured in the Si-detector with the first laser excitation step tuned to a broad bandwidth (nuclear spectroscopy data collection mode). In this mode practically all the hyperfine components are covered by the laser bandwidth and therefore all the isomeric states in ^{185}Pb could be simultaneously ionised, irrespective of the nuclear spin. The spectrum in fig. 2 is dominated by the α-decays of ^{185}Hg ($E_\alpha = 5653(5)$ keV) and ^{185}Tl ($E_\alpha = 5975(5)$ keV) [7]. The latter isotope is abundantly (non-resonantly) produced by surface ionisation in the hot cavity because of its rather low ionisation potential of 6.11 eV. Additionally, ^{185}Tl can be produced via EC/β^+-decay of ^{185}Pb. The nucleus ^{185}Hg is in practice not surface ionised because of its high ionisation potential of 10.44 keV. We assume that in our case ^{185}Hg is produced via EC/β^+-decay of ^{185}Tl, which according to systematics is expected

Table 1. Summary of the previous data and our results on the α-decay characteristics of ^{185}Pb. Shown are α-decay energies E_α, relative intensities I_α, half-life values $T_{1/2}$, hindrance factors HF, coincident γ-rays and isomer assignments. An estimate of $b_\alpha = 50(25)\%$ for the α-branching ratios of both isomeric states in ^{185}Pb was used to calculate hindrance factors (see, subsect. 4.2.1). The artificial lines (6340(20) keV and 6540(20) keV), produced by the summing of energy signals of coincident α-particles and conversion electrons in the Si-detector, are shown in brackets (subsect. 4.2.3).

Ref. [1]		Ref. [2]			Our data					
E_α (keV)	I_α (%)	E_α (keV)	I_α (%)	$T_{1/2}$ (s)	E_α (keV)	I_α (%)	$T_{1/2}$ (s)	HF	Coinc. γ (keV)	Assignment I^π, Isomer
		6290(15)	12(2)	3.9(6)	6288(5)	56(2)	6.3(4)[a]	1.5(8)	205(1), 269(1)	$3/2^-$, ^{185m2}Pb
		6340(15)	15(2)	4.7(8)	(6340(20))	9(2)[b]				sum α-e$^-$ + ^{186}Pb
6400(10)	≈ 72	6406(15)	52(5)	3.6(3)	6408(5)	100	4.3(2)	1.7(9)		$13/2^+$, ^{185m1}Pb
6480(20)	≈ 28	6485(15)	18(3)	6.1(11)	6486(5)	44(2)	6.3(4)[a]	11(6)		$3/2^-$, ^{185m2}Pb
		6535(20)	3(1)	3.5(7)	(6540(20))	6.5(15)[c]				sum α-e$^-$
				4.1(3)[d]						

[a] Deduced from the combined statistics for the 6288 keV and 6486 keV α lines.
[b] Relative to the intensity of the 6288 keV α line.
[c] Relative to the intensity of the 6486 keV α line.
[d] Adopted value from wide α-decay energy interval [2].

to have a dominant EC/β^+-decay branch with a small α-branching ratio. Finally, the nucleus ^{181}Hg, the daughter product of ^{185}Pb after the α-decay, has its strongest α line at $E_\alpha = 6005(4)$ keV and also contributes to the region around 6000 keV in fig. 2. Due to the different possible origins and incomplete knowledge of the α-branching ratios for some of these nuclei, we cannot reliably disentangle the contributions from the different sources in this region of the α spectrum.

In contrast to Tl nuclei, Pb isotopes are poorly surface ionised due to their relatively high ionisation potential of 7.42 eV and the presence of their α-decays in fig. 2 can be explained only by the resonance ionisation in the RILIS. Figure 2 clearly shows the three previously known strongest α lines of ^{185}Pb (see table 1) with the energies of $E_\alpha = 6288(5)$ keV, $E_\alpha = 6408(5)$ keV and $E_\alpha = 6486(5)$ keV. Two other known weaker peaks or shoulders with estimated centroids at $E_\alpha = 6340(20)$ keV and $E_\alpha = 6540(20)$ keV were observed as well (not seen in fig. 2 because of the scale chosen) and will be discussed in detail in subsect. 4.2.3. In this respect our data confirm the results of [2], although, a different assignment will be given both to the three strongest α lines and to the latter two α transitions (sect. 4). The deduced data, along with the previously known ones are shown in table 1 and will be discussed in the following sections.

In the broad-bandwidth mode the total yield of ^{185}Pb was about 1100 ions per μC, assuming the α-branching ratios of 50 % for both isomeric states (see sect. 4).

3.1 Hyperfine structure measurement

As was mentioned in the introduction, the appearance of high-spin and low-spin isomeric states in ^{185}Pb could be expected, similar to the case of the neighbouring nucleus ^{187}Pb [8,9]. In our study the search for isomeric states was performed by carrying out the measurement of the hyperfine structure of the atomic levels.

Coupling of the electronic (J) and nuclear (I) angular momenta leads to a splitting of an atomic level into a number of hyperfine structure components of the total spin $F = I + J$. Figure 1 shows the possible HFS components for the cases of the expected $I^\pi = 13/2^+$ and $I^\pi = 3/2^-$ isomeric states in ^{185}Pb. Because of electronic angular-momentum values of $J = 0$ for the $6p$ ground state and $J' = 1$ for the $7s$ excited state, populated in this work (fig. 1), one and three hyperfine components, respectively, are expected in the ground state (atomic angular momentum F) and in the excited state (atomic angular momentum F'). Therefore, in both cases three atomic transitions are possible between the HFS components of the angular momenta F and F' with difference in their relative positions and amplitudes. If the hyperfine splitting of two isomers differs significantly, tuning of the laser wavelength (frequency) allows to ionise preferentially one of the isomers, *i.e.* to perform isomer separation. Some examples of the application of this method can be found in [12–14].

The measurement was carried out by changing the frequency of the first excitation step (see fig. 1) to tune the laser to the different atomic transitions, while monitoring the yield of different α lines of ^{185}Pb in the Si-detector. For this purpose the first laser excitation step was switched to a narrow-bandwidth mode (1.2 GHz before frequency doubling) with the laser power reduced to decrease the power broadening. In total about 20 subsequent measurements, each lasting on average 300 s, were performed covering the frequency region of interest (about 30 GHz). In this mode the total yield of ^{185}Pb was about a factor of two lower compared with the broad-bandwidth mode.

The stability of the target release, proton beam intensity and laser power are key factors while performing such measurements. The stability of the target and the proton beam intensity were easily monitored by observing the intensity of the non-resonantly produced ^{185}Tl and ^{185}Hg isotopes, see fig. 2. Unfortunately, in our experiment due to a technical problem we could not control the stability of the laser power. Therefore, the peak intensities in the

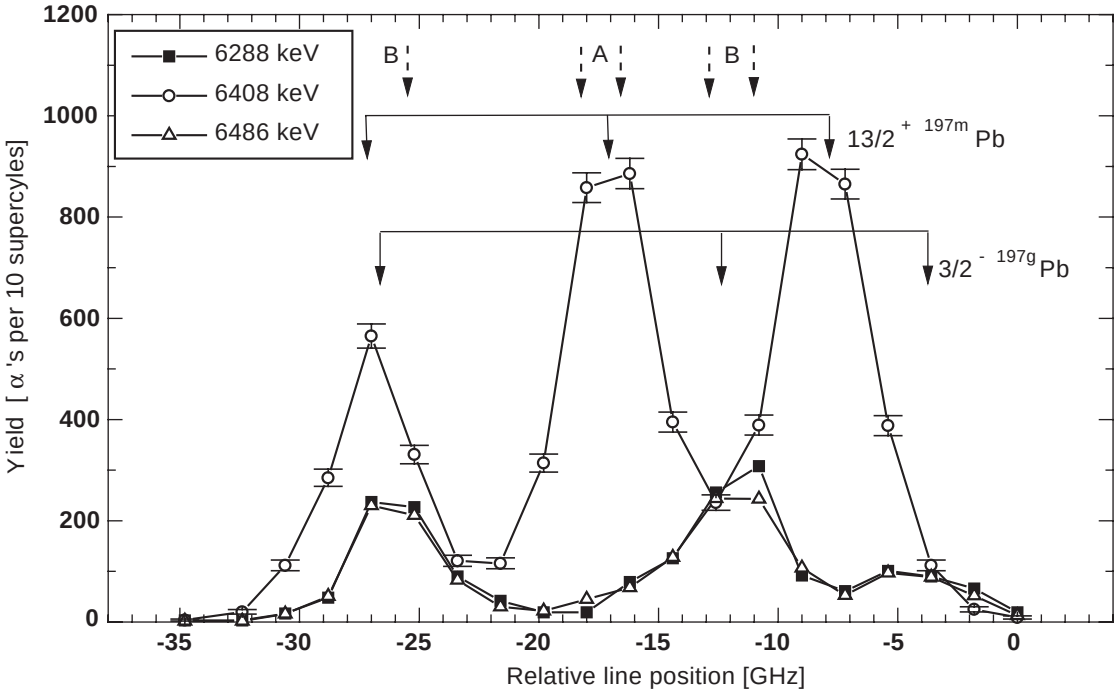

Fig. 3. Yield of different α-decays of ^{185}Pb as a function of the first excitation step laser frequency. The uncertainty of the laser frequency setting in all points is 300 MHz (not shown). For simplicity, the statistical error is shown for the case of the 6408 keV α line only. Dashed arrows with symbols "A" and "B" show the measurements which were further used to produce fig. 4a, b. Full lines with arrows show the positions of the HFS components for the $13/2^+$ and $3/2^-$ isomeric states in ^{197}Pb, taken from [15].

obtained scans may be not fully reliable, but the measured *intervals* between the HFS components for both isomers are less dependent on the laser power stability and should therefore be valid within the laser frequency setting uncertainty and statistical error of the peak.

Figure 3 shows the frequency scan plot: the yield of the three strongest α lines of ^{185}Pb as a function of transition frequency in the first excitation laser step. Despite the Doppler broadening in the hot cavity of the RILIS ($\approx$ 2 GHz at 2100°C for ^{185}Pb) it was still possible in our experiment to resolve the HFS transitions. Three HFS components are observed in all cases and the spectrum clearly demonstrates the different behaviour of the curves, measured for the α line at $E_\alpha = 6408$ keV on the one hand and of the α lines at $E_{\alpha 1} = 6288$ keV and $E_{\alpha 2} = 6486$ keV on the other, which exhibit a very similar pattern.

In order to enhance the observation of different α lines of ^{185}Pb, α spectra collected at specifically chosen frequencies from fig. 3 are shown in fig. 4a, b. Figure 4a shows a part of the α spectrum, summed from the measurements at two neighbouring frequencies, marked by the dashed arrows with the symbol "A" in fig. 3. The measurements at these frequencies clearly enhance the production of the $E_\alpha = 6408$ keV α line of ^{185}Pb. Figure 4b shows a sum α spectrum collected at three frequencies, marked by the dashed arrows with the symbol "B" in fig. 3, which were chosen to enhance the yield of the $E_{\alpha 1} = 6288$ keV and $E_{\alpha 2} = 6486$ keV α lines of ^{185}Pb. We also note the occurrence of high-energy shoulders for both of the latter peaks (at $E_\alpha = 6340(20)$ keV and $E_\alpha = 6540(20)$ keV, respectively, see fig. 4b). The α-decays with similar energies were also identified in [2] (see table 1). Finally, we mention a weak α peak at $E_\alpha = 6455(20)$ keV in fig. 4b, which is not present in fig. 4a. This indicates, that the decay at $E_\alpha = 6455(20)$ keV originates, most probably, from the same state as the decays at $E_{\alpha 1} = 6288$ keV and $E_{\alpha 2} = 6486$ keV. This weak peak is also present in the spectrum measured with a broad-bandwidth laser setting. However, the low statistics and relatively high background do not allow us to make any definite conclusion on the origin of this peak.

Based on the different behaviour of the α lines in fig. 3, we are able to identify, for the first time, two isomeric states in ^{185}Pb: ^{185m1}Pb with an α-decay energy of $E_\alpha = 6408(5)$ keV and ^{185m2}Pb with two α-decays of $E_{\alpha 1} = 6288(5)$ keV and $E_{\alpha 2} = 6486(5)$ keV.

3.2 Spectroscopic data collection and decay scheme of ^{185}Pb

The spectroscopic data were mainly collected by switching the first laser excitation step to the broad bandwidth (10 GHz before the frequency doubling) and full laser power. During approximately 2 hours of data collection about 5×10^3 α-particles were recorded for each of the 6288 keV and 6486 keV decays and about 2×10^4 for the 6408 keV decay of ^{185}Pb, see fig. 2. These data were used for half-

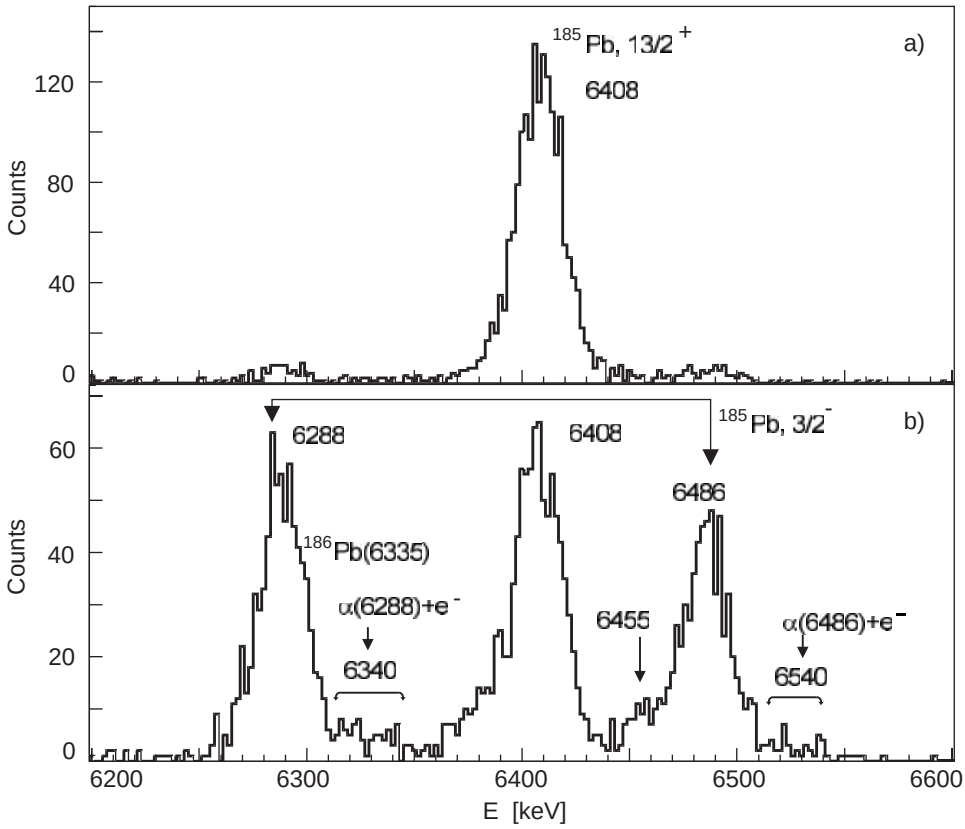

Fig. 4. a) Singles α-energy spectrum summed from the measurements with a narrow bandwidth at the two neighbouring frequencies, marked by the dashed arrows with the symbol "A" in fig. 3; b) The same as a), but summed from the measurements at three frequencies, marked by the dashed arrows with the symbol "B" in fig. 3. Some of the α peaks are labelled with the α-decay energy (in keV) and the isotope the α-decay belongs to.

life determination of the isomeric states and for detailed spectroscopic study.

Figure 5 shows the decay parts of the grow-in/decay curves derived from the TDC spectra with gates on the three strongest α-decays of ^{185}Pb. By fitting the decay part of the TDC curve a half-life value of $T_{1/2} = 4.3(2)$ s for the $E_\alpha = 6408$ keV decay was deduced. The half-life values for the $E_{\alpha 1} = 6288$ keV and $E_{\alpha 2} = 6486$ keV decays are consistent with each other (see fig. 5) and a half-life value of $T_{1/2} = 6.3(4)$ s was derived based on the summed statistics for these two α lines. Therefore, the half-life measurements also confirm the existence of two isomeric states in ^{185}Pb.

Figure 6 shows the energy spectrum of γ-rays, observed in prompt ($\Delta T(\alpha\text{-}\gamma) < 100$ ns) coincidence with the $E_{\alpha 1} = 6288$ keV decay of ^{185m2}Pb. Two previously unknown γ-decays at $E_{\gamma 1} = 205(1)$ keV and $E_{\gamma 2} = 269(1)$ keV, along with the K X-rays of Hg can be seen in this spectrum. No prompt or delayed γ-rays were observed for the 6408 keV and 6486 keV α lines.

Based on these data, the decay schemes of ^{185m1,m2}Pb shown in fig. 7a were constructed. The nucleus ^{185m1}Pb decays by a single α transition to its daughter ^{181}Hg, as no coincident γ or X-rays were observed for the 6408 keV α line. The decay of ^{185m2}Pb is more complex and proceeds via two α-decays. The 6288 keV–269 keV α-γ coincidences establish a previously unknown excited state at 269 keV in the daughter nucleus ^{181}Hg, which presumably decays to the known $1/2^-$ state in this nucleus. Furthermore, the excited state at 269 keV also decays by a 205 keV transition, establishing a new excited state at 64(1) keV in ^{181}Hg. The sum Q_α-value of $Q_{\alpha,\mathrm{sum}} = Q_\alpha + E_\gamma = 6632(5)$ keV for the 6288 keV–205 keV α-γ coincident pairs matches the value of $Q_\alpha = 6629(5)$ keV for the $E_{\alpha 2} = 6486(5)$ keV decay. This means that both the 6486 keV and 6288 keV–205 keV decays feed the same excited level at 64(1) keV in the daughter ^{181}Hg, see fig. 7a. No decay from the excited state at 64 keV was observed in our data.

4 Discussion

4.1 Atomic spectroscopy data for ^{185}Pb

4.1.1 I^π and magnetic moment assignments for the isomeric states in ^{185}Pb

Each experimental HFS curve in fig. 3 was fitted by three Gaussians with fixed widths to determine the peak positions. The error of the peak position is determined by the combination of the statistical error of the fit and the uncertainty of the laser frequency setting in each point

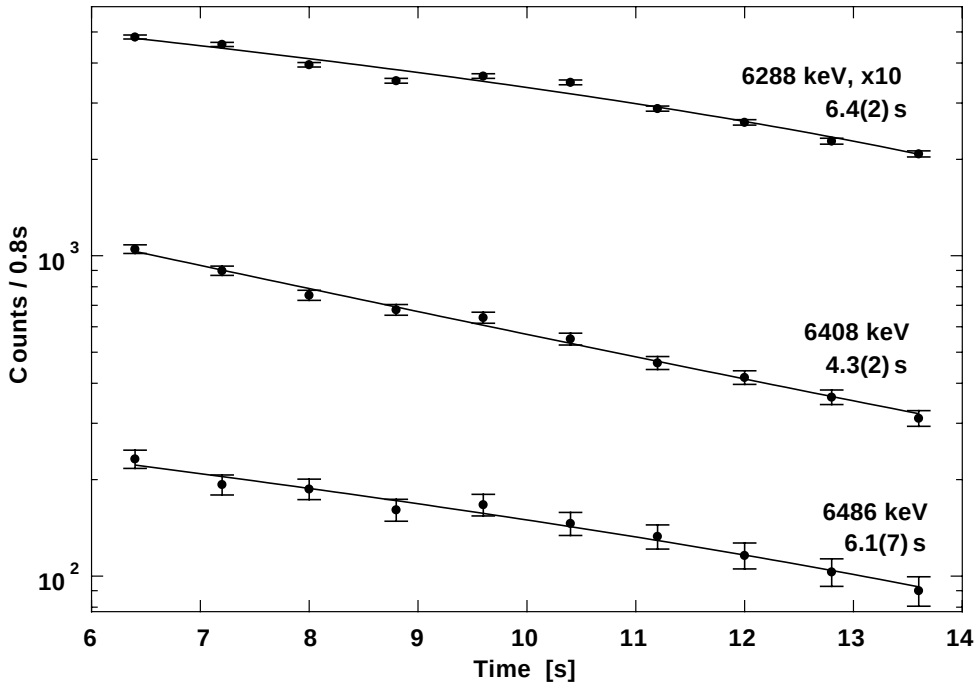

Fig. 5. Decay curves for the three strongest α-decays of ^{185}Pb. The solid lines are the results of the fitting procedure and the deduced half-life values are shown next to each line.

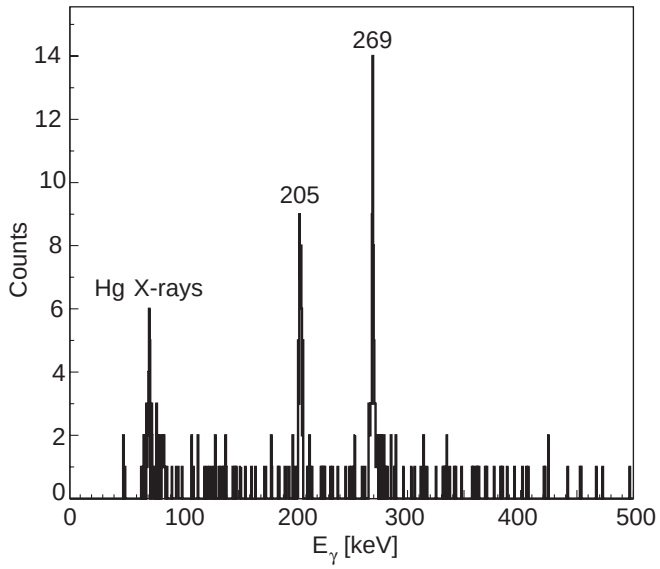

Fig. 6. Energy spectrum of γ-rays observed in prompt coincidence with the α-decay at 6288 keV.

($\approx$ 300 MHz). The hyperfine structure coupling constants A and B and the isomeric shift $\delta\nu(^{185m1,185m2}\mathrm{Pb})$ were extracted from the peak positions according to the well-accepted algorithm (see for example [16]).

The magnetic dipole moments can be evaluated from the scaling relations (see, for example, [3]), based on the known magnetic moment μ_0, magnetic coupling constant A_0 and nuclear spin I_0 of a stable Pb isotope

$$\mu = \frac{A \cdot I \cdot \mu_0}{A_0 \cdot I_0} \,.$$

This expression disregards any hyperfine anomaly, which was found to be less than $\approx 10^{-3}$ for ^{190,191,193,197}Pb isotopes, studied in [3].

The evaluation of the magnetic moment with this method requires knowledge of the nuclear spin I and we considered the spin assignments of $I = 13/2^+$ and $3/2^-$ which are expected from the systematics.

The obtained results are summarized in table 2 and will be discussed below and in the next subsection.

Figure 3 shows that the measured intervals between the HFS components for the assumed $I^\pi = 3/2^-$ isomeric state in ^{185}Pb, decaying by the 6288 keV and 6486 keV transitions, fit well within the frequency setting uncertainty to those for the known $3/2^-$ states in ^{197g,199g}Pb [15]. The HFS intervals for these states in ^{197g,199g}Pb are very similar and for simplicity in fig. 3 we show the data for ^{197g}Pb only. These data were normalized at the position of the assumed $F' = 5/2$ component (left peak in the curves in fig. 3, corresponding to the 6288 keV and 6486 keV decays). Correspondingly, the deduced experimental value for the magnetic moment ($\mu = -1.10(4)\ \mu_N$) is quite similar to the known magnetic moments for the $3/2^-$ ground states in ^{197,199}Pb ($-1.075(2)\ \mu_N$ and $-1.0742(12)\ \mu_N$, respectively [17]). On these grounds, the spin and the parity of $I^\pi = 3/2^-$ were assigned to this isomeric state in ^{185}Pb.

A similarly good agreement can be noted between the measured positions of the HFS components for the assumed $13/2^+$ isomeric state in ^{185}Pb, decaying by the 6408 keV transition, and for the known $13/2^+$ isomeric states in the heavier odd-mass lead nuclei $^{191\text{-}197}$Pb (see fig. 3), where only ^{197m}Pb [15] is shown as a typical example. The deduced magnetic moment for this state ($\mu = -1.19(3)\ \mu_N$) follows, within the error bars, the

Table 2. Hyperfine coupling factors A and B, and nuclear magnetic dipole moments μ for the isomeric states of ^{185}Pb, identified in this work. Isomeric shift $\delta\nu$ and variations of the mean square charge radius $\delta\langle r^2\rangle$ and deformation $\delta\langle\beta^2\rangle$ for the $3/2^-$ isomer were calculated relative to the $13/2^+$ isomer.

I^π	A (MHz)	B (MHz)	μ (μ_N)	$\delta\nu$ (MHz)	$\delta\langle r^2\rangle$ (fm^2)	$\delta\langle\beta^2\rangle$
$3/2^-$	$-5460(150)$	$-120(270)$	$-1.10(4)$	570(300)	0.028(15)	0.0024(13)
$13/2^+$	$-1360(32)$	200(420)	$-1.19(3)$			

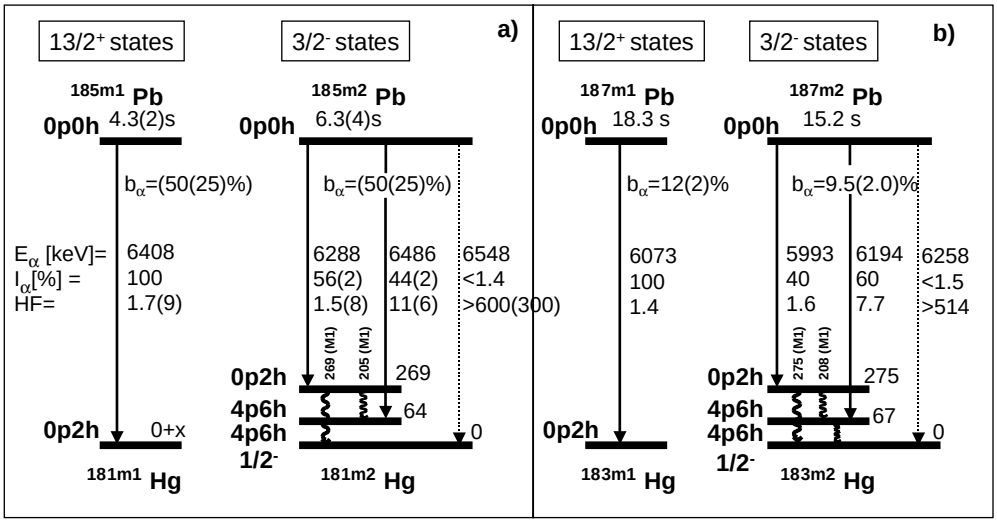

Fig. 7. a) α-decay scheme of ^{185}Pb deduced in this work; b) the same for ^{187}Pb. The data for ^{187}Pb were taken from [7–9,18]. Shown are α-decay energies E_α, intensities I_α, hindrance factor values HF and proton configuration assignments. Estimated α-branching ratios for ^{185m1,185m2}Pb are shown in brackets. Dashed lines with arrows show the possible full-energy α-decays, for which only an upper (lower) limit estimate for the intensity (hindrance factor) values could be deduced. Note, the spin and parity of $I^\pi = 1/2^-$ for the low-spin isomers in ^{181}Hg and ^{183}Hg. The $I^\pi = 3/2^-$ assignment for the excited states in ^{181,183}Hg is tentative and based on the α-decay pattern of parent ^{185,187}Pb nuclei. See main text for details.

nearly constant (or possibly slowly increasing) trend of the known values of the magnetic moments for the $13/2^+$ isomers in ^{191,193,195,197}Pb ($\mu(^{191}\text{Pb}) = -1.172(7)\ \mu_N$, $\mu(^{193}\text{Pb}) = -1.150(7)\ \mu_N$, $\mu(^{195}\text{Pb}) = -1.1318(13)\ \mu_N$, $\mu(^{197}\text{Pb}) = -1.1045(27)\ \mu_N$ [17]). Based on these data, the spin and the parity of $I^\pi = 13/2^+$ were assigned to this isomeric state in ^{185}Pb.

We point out that such nearly constant (within 10%) values of experimental magnetic moments for the $3/2^-$ and $13/2^+$ isomeric states in ^{185}Pb are in a qualitative agreement with the Schmidt estimate of constant $\mu = -1.91\ \mu_N$ for the $p_{3/2}$ and $i_{13/2}$ single-particle neutron states. Despite the quantitative difference of about 40%, which was discussed in the literature for some nuclei close to ^{208}Pb (*e.g.*, [19] and references therein), such constant behaviour of the magnetic moments strongly suggest rather pure single-particle character of the $13/2^+$ and $3/2^-$ isomeric states in ^{185}Pb.

To conclude this part, the data from the HFS scan, despite relatively large experimental uncertainty, determine the spin (and, tentatively, parity) assignments of $I^\pi = 13/2^+$ and $I^\pi = 3/2^-$ for the two α-decaying isomeric states in ^{185}Pb (see table 1). Thus, ^{185}Pb becomes the lightest lead isotope for which the spin and magnetic moment have been deduced experimentally.

4.1.2 Change in charge radius and deformation in ^{185m1,185m2}Pb

The measured isomeric shift value $\delta\nu(^{185m1,185m2}\text{Pb})$ can be used to deduce the mean square charge radius variation $\delta\langle r^2\rangle$, which further provides information on the possible deformation change between the isomers.

The isomeric shift $\delta\nu$, being the displacement of the centres of gravity of the two HFS spectra [16], defines the mean square charge radius variation $\delta\langle r^2\rangle$ as

$$\delta\nu = F \cdot \delta\langle r^2\rangle\,,$$

where the electronic factor $F = 20.26(18)$ GHz/fm^2 was taken from [16]. The deduced value of $\delta\langle r^2\rangle = 0.028(15)$ fm^2 for ^{185m1,m2}Pb (table 2) can be compared to $\delta\langle r^2\rangle = 0.030(7)$ fm^2 [17] for the difference between the $3/2^-$ and $13/2^+$ isomeric states in ^{197}Pb. The latter isotope is the only lead isotope for which the values of $\delta\langle r^2\rangle$ are know for both long-lived isomeric states.

Furthermore, based on the deduced $\delta\langle r^2\rangle$ value, the change in the mean square deformation $\delta\langle\beta^2\rangle$ can be extracted with the well-known prescription (*e.g.*, [3,16])

$$\delta\langle r^2\rangle^{m1,m2} = \delta\langle r^2\rangle_{\rm sph} + \frac{5}{4\pi}\langle r^2\rangle_{\rm sph}\delta\langle\beta^2\rangle^{m1,m2}\,,$$

where $\delta\langle r^2\rangle_{\rm sph}$ and $\langle r^2\rangle_{\rm sph}$ are calculated according to the Droplet-model prescription [20].

By using this method, the value of $\delta\langle\beta^2\rangle^{\rm m1,m2} = 0.0024(13)$ was extracted for ^{185}Pb. This value can be compared to the difference in deformation of $\delta\langle\beta^2\rangle = 0.0025(6)$ between the $3/2^-$ and $13/2^+$ isomeric states in ^{197}Pb. This comparison shows that the value $\delta\langle\beta^2\rangle^{\rm m1,m2}$ is practically the same for ^{185}Pb and ^{197}Pb, despite the fact that the former nucleus has 12 neutrons less than the latter and lies beyond the mid-shell at $N = 104$. This observation further supports the conclusion of the previous subsection, that these states have rather pure single-particle character. Otherwise, the possible admixture of different single-particle and/or of collective excitations could result in a completely different behaviour of deduced $\delta\langle r^2\rangle$ values as is well-known for the neutron-deficient Hg nuclei. To give such an example, we compare the $\delta\langle r^2\rangle^{\rm g,m}$ value for the mean square charge radius change between the $1/2^-$ ground state and $13/2^+$ isomeric state in ^{185,195}Hg. The values of $\delta\langle r^2\rangle^{\rm g,m} = 0.0081(31)$ (^{195}Hg) and $\delta\langle r^2\rangle^{\rm g,m} = 0.4735(23)$ (^{185}Hg) can be deduced from the data given in [16]. This difference clearly reflects the change of the $1/2^-$ ground state from a spherical shell model configuration in ^{195}Hg to a prolate deformed $1/2^-[521]$ Nilsson configuration in ^{185}Hg.

4.2 Alpha-decay data for ^{185}Pb

Before proceeding with the detailed discussion of the measured α-decay data, two comments should be made.

First of all, we stress a striking similarity of the α-decay schemes of ^{185,187}Pb, see fig. 7a, b. In both cases the decay of the high-spin isomers proceeds via a single α-decay to the states in the daughter ^{181,183}Hg, while the decay of the low-spin state proceeds via two α-decays, feeding excited states at a rather close excitation energy in ^{181}Hg (64 keV and 269 keV) and in ^{183}Hg (67 keV and 275 keV). Such a pattern suggests quite similar structures of ^{185,187}Pb and of their respective daughters ^{181,183}Hg. This complementary information was partly used to confirm the spin and parity assignments, based on atomic spectroscopy measurements.

Secondly, our study and available literature data do not provide information on the relative positions of the low-spin and high-spin isomeric states both in ^{185}Pb and its daughter ^{181}Hg. That is why in fig. 7a, as well as in the following discussion, we will denote the high-spin and the low-spin isomers in these nuclei as "m1" and "m2", respectively.

4.2.1 Hindrance factor values and configuration assignments

It is well recognized that α-decay is a powerful tool to identify and study low-lying states giving direct information on the excitation energy, decay pattern and configurations involved (see for examples [9,21]). The latter can be obtained from the α-decay hindrance factor (HF): for example, in odd-mass nuclei a value of HF ≤ 4 means unhindered decay between states of equal spin, parity and configuration [22]. The hindrance factor is defined as the ratio of the reduced α width, calculated by the method of Rasmussen [23], of the transition relative to the reduced α width of the ground state to ground-state transitions in the even-even neighbours.

Unfortunately, in the case of the nucleus ^{185}Pb the calculations of the hindrance factors are somewhat hampered by unknown α-branching ratios for both isomeric states. These branching ratios could not be extracted from our data as the nucleus ^{185}Tl —the daughter of ^{185}Pb after possible EC/β^+-decay is additionally (and more abundantly) produced by the non-resonant surface ionisation (see fig. 2 and discussion in sect. 3) and therefore the direct yield comparison of these two nuclei is not possible. Also, the α lines of the ^{181}Hg nucleus, being the daughter of ^{185}Pb after α-decay, are masked by the α-decays of ^{185}Tl (see fig. 2) and therefore one cannot use the parent-daughter relations to deduce the α-branching ratio of ^{185}Pb. Therefore, in order to obtain an estimate of the branching ratios we used the α-decay systematics for the odd- and even-mass lead nuclei in vicinity of ^{185}Pb. Based on the known α-branching ratios of the following neighbouring nuclei: ≈80% (^{184}Pb [24]), 38(9)% (^{186}Pb [25]), 12(2)% and 9.5(2.0)% ($^{187\rm m1,m2}$Pb, respectively, [9,18]), we derived an estimate of 50(25)% for the α-branching ratios of both isomeric states in ^{185}Pb. Furthermore, an estimate of 50(25)% for the α-branching ratio of the low-spin isomer in ^{185}Pb was suggested in a recent α-decay study of ^{189}Po → ^{185}Pb chain at the velocity filter SHIP [24].

By combining the measured data with estimated α-branching ratios, hindrance factor values shown in table 1 and in fig. 7a were deduced for both isomeric states in ^{185}Pb. The quoted errors of about 50% for the hindrance factors in ^{185}Pb are mainly defined by the uncertainty of the branching ratios.

The HF = 1.7(9) for the 6408 keV α-decay of $^{185\rm m1}$Pb provides experimental evidence for the favoured character of this transition. This fact suggests that the states connected by this decay have the same spin, parity and configuration. Based on the deduced spin value of $I = 13/2$ for $^{185\rm m1}$Pb, this allows us to assign a spin of $I = 13/2$ to the isomeric state in ^{181}Hg to which this transition decays. Based on systematics for the heavier odd-mass lead and mercury nuclei we assume positive parity for both states. We note that recent in-beam work on ^{181}Hg [10] also inferred the existence of a high-spin isomer in ^{181}Hg with a tentative spin and parity assignment of $I^\pi = (13/2^+)$.

Within the spherical shell model approach, the closed shell even-mass lead nuclei can be represented as having a spherical π(0p-0h) configuration, while the even-mass mercury nuclei ($Z = 80$) with two holes in the closed proton shell at $Z = 82$ are represented by a weakly oblate π(0p-2h) configuration. Therefore, we conclude that the 6408 keV α transition directly connects a state in $^{185\rm m1}$Pb, in which the $i_{13/2}$ neutron is weakly coupled to the spherical π(0p-0h) even-even lead core with a state in the daughter $^{181\rm m1}$Hg in which the $i_{13/2}$ neutron is weakly coupled to

a slightly oblate π(0p-2h) even mercury core (see fig. 7a). Such a transition is a normal one-step α-decay, removing a pair of protons from the closed shell at $Z = 82$, and therefore it should not be hindered. The same explanation was given for the 6073 keV α-decay of ^{187}Pb, which also has a relatively small hindrance factor (see fig. 7b and [9,18]).

The decay of the $I = 3/2$ isomeric state in ^{185}Pb is more complex and is split into two transitions. An almost unhindered transition with 6288 keV (HF = 1.5(8)) suggests the same spin of $I = 3/2$ and the same parity for the excited state at 269 keV in ^{181m2}Hg. Based on systematics for the heavier odd-mass lead and mercury nuclei we assume negative parity for the low-spin isomeric state in ^{185}Pb and for the state at 269 keV in ^{181m2}Hg. By analogy with the ^{187m2}Pb case (fig. 7b), we assume that the $3/2^-$ state in ^{185}Pb has a configuration in which the $3p_{3/2}$ neutron is weakly coupled to the spherical π(0p-0h) even-even lead core. This state decays to an excited $3/2^-$ state at 269 keV, originating from the coupling of a $3p_{3/2}$ neutron to a slightly oblate π(0p-2h) even-mass Hg core. As in the case of the $13/2^+$ state this is also a one-step α-decay which is practically unhindered.

The $1/2^-$ isomeric states of ^{181,183}Hg are known to result from the coupling of the $3/2^-$ neutron to a prolate even-mass core, which yields (see fig. 7a,b) a $1/2^-$ state as the lowest state of the band [26,27]. Such a configuration can be described in the spherical shell model approach as a π(4p-6h) excitation which lies lower in energy than the state originating from the weak coupling of the $3/2^-$ neutron to the slightly oblate core of π(0p-2h) character (the state at 269 keV), although the latter configuration is the lowest one in the even-even mercury neighbours. Within the multiparticle-multihole approach an α-decay between the spherical π(0p-0h) configuration in ^{185}Pb and prolate π(4p-6h) configuration in ^{181}Hg should be strongly hindered as it involves a multi-step process. This is in agreement with non-observation of the possible $3/2^- \rightarrow 1/2^-$ 6548 keV direct α decay to the $1/2^-$ state in ^{181}Hg, which is shown in fig. 7a by the dashed line. To give a quantitative estimate for this hindrance, we use the assumption of an upper limit of $\approx 1.4\%$ (see subsect. 4.2.3) for the intensity of this decay relative to all α-decays from the same state. Under this assumption a hindrance factor of HF $\geq$ 600(300) for the possible 6548 keV transition can be obtained. This is similar to the case of ^{187}Pb, in which no direct $3/2^- \rightarrow 1/2^-$ decay with $E_\alpha = 6258$ keV was observed as well, see fig. 7b. Based on the quoted upper limit of 1.5×10^{-2} [8] for the intensity of this transition, a lower limit for the hindrance factor value of HF > 514 can be derived for the possible 6258 keV transition in ^{187}Pb.

The excited state at 64 keV can be interpreted as the $3/2^-$ member of the rotational band, built on top of the $1/2^-$ isomeric state. This assumption is supported by the systematics of the excited $3/2^-$ states in the $N = 101$ isotones, shown in fig. 8, and by the estimated multipolarity of the 64 keV transition (see next subsection). Then, in the absence of other effects, one of them being the mixing with the closely lying states of the same spin and parity, one would expect the α-decay to the band head and to the first excited state within the band with $\Delta I = 1$ to be hindered to a similar extent. This is not the case in ^{185}Pb nor in ^{187}Pb (see fig. 7a,b): the decay to the assumed $3/2^-$ member of the $\Delta I = 1$ band is not completely forbidden in both cases and points to some mixing between the two $3/2^-$ states in ^{181}Hg and also in ^{183}Hg.

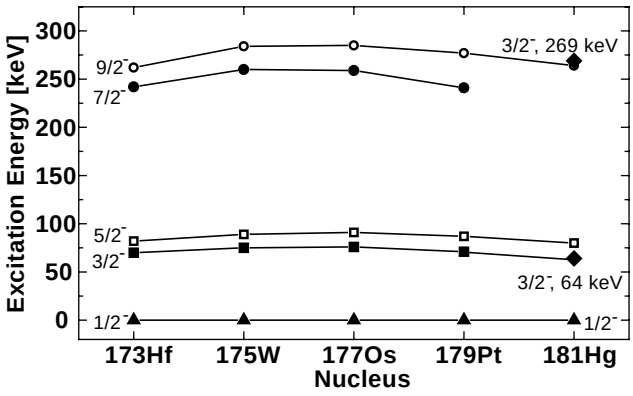

Fig. 8. Systematics of some lowest members of the prolate rotational band, built on the $1/2^-[521]$ Nilsson orbital in the $N = 101$ isotones. The data for ^{181}Hg are taken from [10] and from this study. The tentative $3/2^-$ excited states in ^{181}Hg, identified in this work, are shown by the filled diamonds and denoted with their excitation energies (in keV). The rest of the data is taken from [7].

4.2.2 Multipolarity estimates for the 64 keV, 205 keV and 269 keV γ transitions

The $I^\pi = 3/2^-$ spin and parity assignments for the excited states at 64 keV and 269 keV in ^{181}Hg are also in agreement with the following multipolarity estimates for the 205 keV and 269 keV γ transitions. We note that the prompt character of these transitions limits their multipolarity to $E1$, $E2$ or $M1$. One can further give an estimate for the conversion coefficients for these transitions by assuming two different scenarios for the origin of the observed K X-rays in fig. 6. As a first possibility we assume that the observed K X-rays result solely from the conversion of the 205 keV decay. Then, by comparing the number of observed K X-rays and 205 keV decays in fig. 6, after correction for corresponding experimental X-ray and γ efficiencies, a conversion coefficient of $\alpha_K = 1.2(3)$ can be deduced for this transition. This points to the $M1$ character of this transition, as the calculated conversion coefficients for the 205 keV γ-decay are as follows: $\alpha_K(M1) = 0.88$, $\alpha_K(E2) = 0.4$, $\alpha_K(E1) = 0.06$ [28]. In the second scenario we consider the possibility that the observed K X-rays in fig. 6 result from the conversion of the 269 keV decay only. In this case, by applying the same procedure as above for the 205 keV decay, a conversion coefficient of $\alpha_K = 0.65(15)$ can be deduced for the 269 keV transition. This value should be compared to the calculated values of $\alpha_K(M1) = 0.4$, $\alpha_K(E2) = 0.08$, $\alpha_K(E1) = 0.03$, which speaks in favour of $M1$ multipolarity assignment for this transition. However, one can see

that in both cases, the experimentally deduced conversion coefficient is always somewhat larger than the corresponding calculated value of $\alpha_K(M1)$. This fact suggests that the K X-rays in fig. 6 originate from the conversion of both 205 keV and 269 keV transitions and we therefore suggest that these transitions should be assigned as being of an $M1$ multipolarity, although a mixed $M1/E2$ multipolarity assignment for one or both of them cannot be excluded. This is consistent with the tentative assignment of an $M1$ multipolarity to the 208 keV and 275 keV transitions in ^{183}Hg [8].

An $E1$ multipolarity for any of these γ transitions can be ruled out based on a number of arguments. First of all, the theoretical K-conversion coefficients for the 205 keV and 269 keV γ transitions of $E1$ multipolarity are very small (see above). Secondly, such an assignment would require a parity change for either the 64 keV state or 269 keV state, which will be difficult to reconcile with the hindrance factor values for corresponding feeding α-decays and with the results of the in-beam study [10].

As was discussed above, we tentatively assign spin and parity of $3/2^-$ (see fig. 7a) to the excited state at 64 keV in ^{181}Hg, which then can decay via $M1$ or $E2$ transitions (or their mixture) to the $1/2^-$ isomeric state. To put the spin assignment on a stronger footing a lower limit for the conversion coefficient for the (unobserved) 64 keV decay can be deduced from our data. Assuming an upper limit of ≤ 1 count for the number of the 6288 keV–64 keV α-γ coincidences and using the number of 6288 keV–205 keV decays, corrected for the conversion coefficient for the 205 keV decay and for the ratio of the γ-efficiencies for the 64 keV and 205 keV decays, a lower limit of $\alpha_{\rm tot}(L) \geq 21$ for the total L-conversion coefficient for the 64 keV decay can be obtained. This should be compared to the total theoretical L-conversion coefficients for the 64 keV transition of $4.2(M1)$ and $32(E2)$, respectively [28]. This suggests that the 64 keV transition in ^{181}Hg should be preferentially assigned as being of a rather pure $E2$ multipolarity, although some mixing with the $M1$ multipolarity can not be excluded. This is similar to the case of ^{183}Hg, in which a strongly converted ($\alpha = 26 \pm 4$) prompt pure $E2$ or possibly mixed $M1/E2$ 67 keV transition, decaying directly to the $1/2^-$ isomeric state was found [8] (see fig 7b).

To conclude the two previous subsections, we point out that complementary data from the HFS measurements and from the α-decay data are fully consistent to each other and provide unique assignment for the spins and parities of the states, studied in ^{185}Pb and ^{181}Hg.

4.2.3 Interpretation of the 6340 keV and 6540 keV α-decays of ^{185}Pb

The strongly converted 64 keV transition in ^{181m2}Hg has direct relevance to the appearance of the low-intensity peaks or shoulders with estimated centroids at 6340(20) keV and 6540(20) keV in our α-decay data, see table 1 and fig. 4b.

First of all, we note the same energy difference of about 50 keV in the pairs of 6288 keV–6340 keV and 6486 keV–6540 keV α-decays. This energy difference corresponds, within the error bars, to the energy of the conversion electrons which would result from the L-conversion of the 64 keV transition in the daughter ^{181}Hg, see fig. 7a ($E_{e^-} = 64$ keV $- B_{e^-} \approx 50$ keV, where B_{e^-} is the binding energy of the L-electrons in Hg [7]). Therefore, we suggest that the α peaks at 6340(20) keV and 6540(20) keV are artificial peaks, resulting from the full summing in the Si-detector of the energy of the 6288 keV and 6486 keV decays, respectively, with the L-conversion electrons from the 64 keV transition.

Such an effect was already discussed in [8] for ^{187}Pb, for which an artificial α line with $E_\alpha = 6258$ keV was found, presumably caused by summing of 6194 keV α-particles with coincident conversion electrons from the strongly converted 67 keV transition (see fig. 7b).

Clearly, the intensity of such summing peaks depends on the tape–Si-detector geometry, used in the experiment. To check the assumption of α-e$^-$ summing we performed simulations using the GEANT Monte Carlo code [29], taking into account the real geometry of our setup. A reliable upper estimate for the implantation spot size is given by the beam diaphragm of about 6 mm, installed at a rather close distance from the implantation point. The inclination of the beam direction and of the Si-detector relative to the tape were also taken into account. The former resulted in an ellipsoidal beam spot size on the implantation tape.

These simulations showed that in the given geometry, the α-e$^-$ summing efficiency is 3.3 % relative to the detection efficiency for the "pure" α-decay. One should note that the calculated summing efficiency depends rather weakly on the implantation beam spot, increasing only slightly with a decrease of the latter value. Therefore, the calculated summing efficiency should be considered as the lower limit in case the real beam size was smaller than the diaphragm used. One can see, that the calculated value is about a factor of two lower compared with the value of 6.5(1.5)% measured in the experiment for the 6540 keV α line, although the rather large experimental error prevents more definitive conclusions being drawn.

One could try to assign the difference between the experimental and calculated values for the intensity of the 6540(20) keV line as resulting from the direct full-energy $3/2^- \rightarrow 1/2^- \alpha$ transition from the low-spin isomer in ^{185}Pb to the $1/2^-$ state in ^{181}Hg. Such a transition would have an energy of 6548 keV and would not be distinguished from the 6540(20) keV decay. In such a case, an upper limit of $\approx$1.4% for the 6548 keV α-decay relative to *all* α-decays from the low-spin isomer in ^{185}Pb could be deduced. This value was used in subsect. 4.2.1 to calculate a lower limit for the hindrance factor for this transition.

For the α-decay at 6340(20) keV the calculated intensity of 3.3% of the sum α-e$^-$ peak is lower than the experimental value of 9(2)%. However, the α-decay of the neighbouring ^{186}Pb with similar α-decay energy and half-life values ($E_\alpha = 6335(10)$ keV, $T_{1/2} = 4.6$ s [7]) also contributes to the peak at 6340(20) keV. The yield of this isotope was measured shortly before the study of ^{185}Pb

and was found to be about ten times higher than that of ^{185}Pb. Although after mass separation with the GPS tuned to $A = 185$, ^{186}Pb should be suppressed by about 10^{-3} times, because of the yield difference the α-decays from ^{186}Pb will be suppressed to a level of "only" $\approx 10^{-2}$ relative to those of ^{185}Pb. Therefore, with all the uncertainties in the yield and mass separation efficiency estimates we consider the agreement between the experimental and calculated intensity for the 6340(20) keV α-decay to be satisfactory within the error bars.

Most probably the same effect can explain the appearance of these peaks in a previous study [2], in which mass separation and implantation in a tape, surrounded by Si-detectors was also applied. In ref. [1] no such α lines were mentioned, but also the much stronger peak at 6288 keV was not attributed to ^{185}Pb at all.

Finally, we would like to discuss the weak α peak at 6455(20) keV in fig. 4b. As was mentioned in subsect. 3.1, this peak is only present in the measurements with the laser frequency chosen to enhance the production of the low-spin isomer in ^{185}Pb. On this basis one could tentatively assign this α-decay as belonging to this isomer. In such a case, this would establish an excited state at about 97(15) keV in the daughter ^{181m2}Hg. However, due to low statistics and a relatively high background we prefer not to make any definitive assignment for this peak.

4.2.4 Excited states in ^{181}Hg: comparison with in-beam data

Before this work, excited states in ^{181}Hg were investigated in α-decay studies of ^{185}Pb [1,2] and in a recent in-beam study [10]. In particular, in ref. [10] a few prolate rotational bands were identified, presumably based on the $1/2^-[521]$ orbital from the $3p_{3/2}$ sub-shell, $5/2^-[512]$ orbital from the $1h_{9/2}$ sub-shell and $7/2^+[633]$ orbital from the $1i_{13/2}$ sub-shell. Also, an indication on the existence for an oblate (presumably $13/2^+$) isomeric state was presented.

It is interesting to note that the two new excited states at 64 keV and at 269 keV, clearly observed in our study in ^{181}Hg, were not seen in [10] and, conversely, no decays to the excited states observed in [10] were found in our study. As suggested in [10], the lowest observed excited state above the $1/2^-$ prolate band head is presumably the $5/2^-$ state at an excitation energy of 81 keV, decaying possibly by an $E2$ transition to the band head. This assignment was *partly* based on the previous α-decay studies [1,2]. The authors of [10] assumed that the only isomeric state known at that moment in ^{185}Pb decays by the 6400 keV and 6480 keV α transitions to two states leading to the *same* isomer in the daughter ^{181}Hg. On these grounds the conclusion was drawn in [10] that an excited state at 80 keV exists in ^{181}Hg and some evidence was suggested for a 80.5 keV γ-decay, presumably de-exciting this level.

In this respect we stress that, first of all, no suggestion of the existence of an excited state at 80 keV was made by the authors of the original α-decay studies [1,2]. Secondly, in our work no evidence for an excited state at 80 keV in ^{181}Hg populated by α-decay was found. Finally, we have shown that the α-decays at 6408 keV and 6486 keV proceed from two different isomeric states in ^{185}Pb and populate levels leading to different isomeric states in ^{181}Hg. Therefore, we conclude that, although the $5/2^-$ state at 80 keV might indeed exist in ^{181}Hg, the assumption of [10] for the observation of such a state from the previous α-decay studies is not correct and cannot be used for the justification of the 80 keV excited state in ^{181}Hg.

Nevertheless, this does not rule out that such a state could have been populated in the in-beam study of [10]. Furthermore, there are two obvious experimental reasons why this state could not be seen in our experiment. First of all, we are not able to observe the corresponding α-decay in the singles α spectrum (figs. 2,4), as its energy of $E_\alpha = 6470$ keV would not be distinguished from the much stronger 6486 keV transition. Also, since the 80 keV $E2$ transition should be strongly converted, we would not see such a decay in the α-γ coincident matrix, as in the case of the 6486 keV–64 keV α-γ coincidences.

A stronger argument why this decay could not be observed in our study comes from the assignment in ref. [10] of this state as a member of a prolate rotational band, built on the $1/2^-[521]$ orbital. As mentioned earlier, the α-decays to the band head and to the lowest excited members of the same rotational band have usually quite similar hindrance factor values, differences arising from the angular-momentum change ΔL. As we showed above, the direct 6548 keV α-decay between the spherical $3/2^-$ state in ^{185}Pb and the prolate $1/2^-[521]$ state in ^{181}Hg is strongly hindered (HF $> 600(300)$). According to the Rasmussen prescription [23], the possible 6470 keV $3/2^- \rightarrow 5/2^-$ decay of ^{185}Pb would involve a quite similar hindrance factor and therefore this decay could not be observed as well. The same reason explains, most probably, the non-observation of the α-decays to other low-lying excited states in ^{181}Hg that were observed in the in-beam study [10].

Finally, some speculations on the nature of the 64 keV and 80 keV states in ^{181}Hg could be made. These states could be tentatively interpreted as the signature partners of the prolate rotational band built on the $1/2^-[521]$ orbital. Such an assignment is supported by the similarity with the signature partner $3/2^-$ and $5/2^-$ states that are known in the $N = 101$ isotones of ^{181}Hg: ^{179}Pt, ^{177}Os, ^{175}W and ^{173}Hf [7]. In all these cases a prolate deformed rotational band, built on the $1/2^-[521]$ Nilsson orbital was found with the $3/2^-$ member of the band always lying about 15 keV below the $5/2^-$ member (see fig. 8). The excitation energies of the $3/2^-$ and $5/2^-$ states in all these cases are about 70 keV and 85 keV, respectively, which are quite similar to the values of 64 keV and 80 keV observed in ^{181}Hg. We note that the position of the prolate $3/2^-$ state in ^{181}Hg at 64 keV could be somewhat perturbed by the mixing and interaction with the oblate $3/2^-$ state at 269 keV. However, due to lack of definitive proof, no solid conclusions can be drawn here.

5 Conclusions

The resonance ionisation laser ion source coupled to the ISOLDE mass separator was used to study the mid-shell nucleus ^{185}Pb ($N = 103$). In contrast to previous investigations two long-lived isomeric states were found in ^{185}Pb and their α-decay characteristics were investigated.

Furthermore, based on the hyperfine splitting measurements, nuclear spins and magnetic moments of these isomeric states were deduced. Complementary α-decay data confirm the spin assignments and, based on systematics, the high-spin and low-spin isomers were assigned as having positive and negative parity, respectively, in ^{185}Pb. The magnetic moment of the $13/2^+$ isomer in ^{185}Pb was found to be similar to those of the $13/2^+$ isomers in the heavier odd-mass $^{191\text{-}197}$Pb lead nuclei. The same conclusion can be also drawn by comparing the magnetic moment for the $3/2^-$ isomer in ^{185}Pb with corresponding $3/2^-$ isomeric states in the heavier ^{197,199}Pb.

By using the α-γ coincidence technique, information on new excited states in the daughter ^{181}Hg was obtained. A striking similarity of the decay patterns (*e.g.*, HF values, excitation energies) in the ^{187}Pb $\rightarrow$ ^{183}Hg and ^{185}Pb $\rightarrow$ ^{181}Hg decay chains was found. This fact, along with the literature data, points to the robustness of the configurations involved in these decays: the spherical isomeric configurations in the parent lead nuclei and coexisting weakly oblate and prolate-deformed configurations in the daughter mercury isotopes.

Despite a rather large experimental uncertainty of the values of the magnetic moments and $\delta\langle r^2\rangle$ deduced in this study, the data obtained clearly demonstrate the power of the method used. To put all these data on a stronger footing, a systematic study on the behaviour of the magnetic moments and $\delta\langle r^2\rangle$ values in a longer isotopic chain of lead isotopes is necessary. It would be very important in the future to undertake a similar kind of study, possibly with improved statistics and quality, to bridge the gap between ^{185}Pb and the lightest lead isotope ^{190}Pb, studied by atomic spectroscopy method.

This work was supported by the Access to Large Scale Facility program under the Training and Mobility of Researchers program of the European Union Contract HPRI-CT-1999-00018, by the FWO-Vlaanderen and by the GOA and IUAP program, Belgium. KVdV is Research Assistant of the FWO-Vlaanderen. ANA was partially supported by the EXOTAG project, HPRI-CT-1999-50017.

References

1. C. Cabot *et al.,* Nucl. Phys. A **241**, 341 (1975).
2. U.J. Schrewe *et al.,* Phys. Lett. B **91**, 46 (1980).
3. S.B. Dutta *et al.*, Z. Phys. A **341**, 39 (1991).
4. A.N. Andreyev *et al.*, Eur. Phys. J. A **6**, 381 (1999).
5. V.I. Mishin *et al.*, Nucl. Instrum. Methods Phys. Res. B **73**, 550 (1993).
6. V.N. Fedoseyev *et al.*, Hyperfine Interact. **127**, 409 (2000).
7. R.B. Firestone *et al., Table of Isotopes*, 8th ed. (John Wiley & Sons, Inc., New York, 1996).
8. P. Misaelidis *et al.*, Z. Phys. A **301**, 199 (1981).
9. A.N. Andreyev *et al.*, Phys. Rev. Lett. **82**, 1819 (1999).
10. P.G. Varmette *et al.*, Phys. Lett. B **410**, 103 (1997).
11. U. Köster, Nucl. Phys. A **701**, 441 (2002).
12. V.I. Mishin *et al.*, Opt. Comm. **61**, 383 (1987).
13. U. Köster *et al.*, Hyperfine Interact. **127**, 417 (2000).
14. L. Weissman *et al.*, Phys. Rev. C **65**, 024315 (2002).
15. M. Anselment *et al.*, Nucl. Phys. A **451**, 471 (1986).
16. E.W. Otten, *Treatise on heavy-ion science*, edited by D.A. Bromley, Vol. **8** (Plenum Publishing, 1989).
17. N.J. Stone, *Table of Magnetic Dipole and Electric Quadrupole moments* (Oxford University Physics, Clarendon Laboratory, Oxford, 2001) `http://www.nndc.bnl.gov/nndc/stone_moments`.
18. A.N. Andreyev *et al.*, submitted to Phys. Rev. C (2002).
19. C. Ekström, G. Wannberg, Y.S. Shishodia, Hyperfine Interact. **1**, 437 (1976).
20. W.D. Myers, K.-H. Schmidt, Nucl. Phys. A **410**, 61 (1983).
21. N. Bijnens *et al.*, Phys. Rev. Lett. **75**, 4571 (1995).
22. Nuclear Data Sheets **15**, no. 2, VI (1975).
23. J.O. Rasmussen, Phys. Rev. **113**, 1593 (1959).
24. A.N. Andreyev *et al.*, work in preparation.
25. A.N. Andreyev *et al.*, J. Phys. G. **25**, 835 (1999).
26. J. Bonn *et al.*, Phys. Lett. B **38**, 308 (1972).
27. G. Ulm *et al.*, Z. Phys. A **325**, 247 (1986).
28. Program to calculate conversion coefficients, National Nuclear Data Center (NNDC) `http://www.nndc.bnl.gov/nndc/physco/`.
29. GEANT Detector Simulation Tool, CERN, Geneva, 1993; `http://wwwinfo.cern.ch/asd/geant`.